Korean J. Chem. Eng., 35(4), 974-983 (2018)
DOI: 10.1007/s11814-017-0340-6

pISSN: 0256-1115
eISSN: 1975-7220

Electrochemical synthesis, characterization and application of a microstructure $Cu_3(BTC)_2$ metal organic framework for CO_2 and CH_4 separation

Kasra Pirzadeh, Ali Asghar Ghoreyshi†, Mostafa Rahimnejad, and Maedeh Mohammadi

Chemical Engineering Department, Babol Noshirvani University of Technology, Babol, Iran
(*Received 27 September 2017 • accepted 4 December 2017*)

Abstract−The electrochemical route is a promising and environmentally friendly technique for fabrication of metal organic frameworks (MOFs) due to mild synthesis condition, short time for crystal growth and ease of scale up. A microstructure $Cu_3(BTC)_2$ MOF was synthesized through electrochemical path and successfully employed for CO_2 and CH_4 adsorption. Characterization and structural investigation of the MOF was carried out by XRD, FE-SEM, TGA, FTIR and BET analyses. The highest amount of carbon dioxide and methane sorption was 26.89 and 6.63 wt%, respectively, at 298 K. The heat of adsorption for CO_2 decreased monotonically, while an opposite trend was observed for CH_4. The results also revealed that the selectivity of the developed MOF towards CO_2 over CH_4 enhanced with increase of pressure and composition of carbon dioxide component as predicted by the ideal adsorption solution theory (IAST). The regeneration of as-synthesized MOF was also studied in six consecutive cycles and no considerable reduction in CO_2 adsorption capacity was observed.

Keywords: MOF, $Cu_3(BTC)_2$, Electrochemical Synthesis, CO_2/CH_4 Adsorption, IAST

INTRODUCTION

Capture of CO_2 and CH_4 as the main greenhouse gases has attracted much interest in clean energy researches [1]. Emission of these gases into the atmosphere threatens the environment and life on our planet. Increase of sea levels, floods, droughts, species extinction, and so on are some consequences of global warming caused by emission of greenhouse gases into the atmosphere [2]. In the case of CO_2, carbon capture and sequestration (CCS) is one of the novel approaches to mitigate the carbon dioxide emission and also can protect the environment from global warming hazards. The CCS technology can be divided into three subcategories: (i) CO_2 capture and separation in industries, (ii) compression and transport to injection sites, and (iii) geological storage for further applications [3].

Natural gas is composed of a large amount of methane and considerable quantity of light and heavy hydrocarbons along with other impurities like CO_2, N_2 and H_2S. These compounds must be removed from natural gas since they can cause pipeline corrosion during down/upstream processing due to their acidic nature. Hence, it is necessary to mitigate the quantity of CO_2 in natural gas to 50 ppm [4] for pipeline transportation and liquification and also for improving the heating value of natural gas. Consumption of methane as the main constituent of natural gas is increasing as it generates lower amount of CO and CO_2, as well as NO_x and SO_x, per unit of energy compared to other fossil fuels [5]. However, there are some drawbacks restricting the wide-spread use of natural gas: its low energy density and storage limitations [6].

Among various techniques, such as membrane process, absorption, adsorption and cryogenic methods, for removing acid gases (like CO_2) from raw natural gas stream, the processes based on adsorption have attracted considerable attention due to their simplicity in adsorbent regeneration via thermal or pressure variation [7]. Physical adsorption, specially by microporous materials, is a promising and cost-effective approach for storage and separation of CO_2. Numerous porous materials such as zeolites [8,9], carbon nanotubes [10], nanoporous carbons [11,12], and metal organic frameworks (MOFs) [13,14], have been used for adsorption of CO_2 from fuel/flue streams. Some of these materials suffer from serious shortcomings such as low adsorption capacity, poor selectivity over other gases, low physical or chemical stability [3]. Therefore, finding an appropriate adsorbent to overcome these drawbacks must be the first aim in gas separation and storage studies.

MOFs are a class of crystalline materials that have attracted much attention over the last two decades [15]. These interesting porous materials are formed by strong bonds between the metal clusters or ions and organic ligands. The combination of inorganic and organic species generates a diverse number of combinations which have some salient features such as high adsorption capacity, large specific surface area and high pore volume. In addition, high thermal stability (up to 400 °C), flexible and designable framework, permanent porosity and ability to be functionalized or grafted are some other characteristics of MOFs [16]. Such versatility in design and configuration has led to the wide applications of MOFs in various areas such as catalysis, sensors, fuel cell, drug delivery and gas adsorption and separation [17].

Several routes have been proposed for MOFs synthesis such as solvothermal/hydrothermal [18], sonochemical [19], microwave [20] and electrochemical methods. Solvothermal/hydrothermal method is a conventional synthesis approach which takes some days and

†To whom correspondence should be addressed.
E-mail: aa_ghoreyshi@nit.ac.ir, aa_ghoreyshi@yahoo.com

operates at high pressures and temperatures. In recent years researchers have attempted to find faster routes that produce MOFs with the same characteristics like sonochemical and microwave approaches; however, there are few reports on electrochemical methods. Electrochemical synthesis is a facile and environmentally friendly approach that can produce nanostructure materials, which may be hardly achievable by conventional techniques [21]. In this method, there is more control on the reactant concentration over period of time due to the absence of pressure buildup. In addition, by controlling the anodic oxidation, different rates of metal ions can be added to the solution [22]. On the other hand, rapid synthesis at lower temperatures compared to conventional synthesis methods and no need to metal salts can add to the advantages of the electrochemical synthesis route. This procedure was first pioneered by Muller and coworkers [23] in 2005 when they generated MOFs via electrosynthesis in methanol medium. In this method, instead of metal salt, an electrode supplies the required metal ions for synthesis. Then, the electrode is placed in the solution which contains ligand and is in most cases accompanied by electrolyte. The metals dissolve by applying suitable voltage or current and the released metal ions react with linkers to form MOF near the electrode surface [18].

$Cu_3(BTC)_2$ (also known as HKUST-1) is one of the well-known MOFs first synthesized by Chui et al. in 1999 [24]. This MOF is comprised of Cu^{2+} cluster coordinated by carboxylate groups of 1,3,5-benzentricarboxylate acid as an organic linker to form a paddlewheel unit in which four carboxylate groups form a square (Fig. 1). The Cu^{+2} ion fulfills its lack of electrons through a weak bond and its axial coordination site is occupied by lone pair solvent molecule. Consequently, these building blocks form a three-dimensional cubic framework with open pore system through BTC ligands [25]. Ease of synthesis and chemical stability are considered as the main features making this MOF a suitable candidate for studies [18].

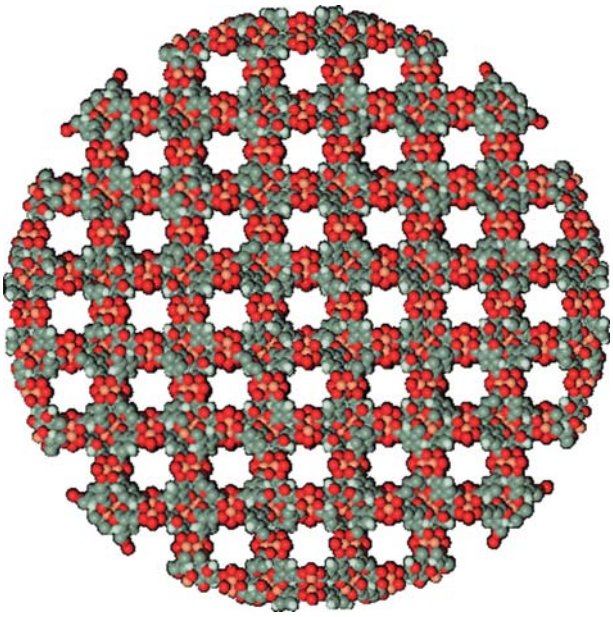

Fig. 1. Molecular structure of $Cu_3(BTC)_2$ (C: gray H: white O: red Cu: orange).

One of the main concerns in researches, especially in engineering, is the commercialization of academic outputs or scaling up the pilot studies for industrial applications. In this regard, utilization of MOFs at large scales, such as gas storage and separations units, is one of the issues that should be addressed. Although numerous studies have been reported about the potential of MOFs in various technological fields, only few academically pure ideas became applicable in reality and daily life [26]. Among very few companies that developed the utilization of MOFs to larger scales, BASF was the first showing interest in MOFs and claims to be the pioneer in production of MOFs on a large scale [23]. This company developed an electrochemical approach to synthesize $Cu_3(BTC)_2$ for industrial purposes since they predicted the technological importance of MOFs, mainly because of their salient properties such as ultra-high specific surface area, tunability and availability and cheap reactants for its synthesis [27]. One of the remarkable and at the same time recent applications of MOFs is in transport industry. Considerable efforts have been made to find solutions for fuel storage, separation and catalysis. Ecofuel Asia Tour (in 2007) was the first project in which MOFs were applied for gas storage. The pellets of $Cu_3(BTC)_2$ were chosen for MOF-tank since it has high capacity for CNG storage [27].

Gas separation is another possible field where MOFs can be beneficially applied at industrial scale. In this process, the gas mixtures are separated with pressure swing adsorption (PSA) or temperature swing adsorption (TSA) methods; however, PSA has some advantages over TSA such as high selectivity, high adsorption capacity and facile adsorbent regeneration [28]. Separation of nitrogen from oxygen (air), nitrogen from carbon dioxide and nitrogen from methane are some of the examples which were previously done by zeolitic adsorbents. The key component in this regard is the price and adsorption capacity of the adsorbent, which plays a significat role in the process economy.

The main objective of this study was synthesizing $Cu_3(BTC)_2$ via electrochemical route, investigating its potential for adsorption of CO_2 and CH_4 and predicting its separtion performance by ideal adsorption theory. Many studies have been done on the adsorption of CO_2 and CH_4 by MOFs which were synthesized by solvothermal method; however, still there is no report on adsorption of these gases on electrochemically synthesized MOFs. The MOF structure was characterized by various analyses such as BET, XRD, FTIR, TGA and FE-SEM. Also, adsorption isotherms and thermodynamic studies were performed using appropriate physical models. IAST was used to model the selectivity of CO_2/CH_4 in the gas mixture from pure component isotherm data. Finally, reusability of the as-synthesized MOF was studied to identify the adsorption uptake stability.

MATERIALS AND METHODS

1. Materials

Cu-plates were chosen as cathode and anode electrodes. 1,3,5 Benzentricarboxylate acid (H_3BTC, Merck, Germany), Tetrabutylammoniumtetrafluoroborate (TBATFB, Sigma, USA) and ethanol (Merck, Germany) were used as ligand, supporting electrolyte

and solvent, respectively.

2. MOF Synthesis

Two copper electrodes with similar area (8 cm^2) were placed in an electrolysis cell which contained 100 ml ethanol solution. 1 g H_3BTC and 0.65 g TBATFB as supporting electrolyte were dissolved in 100 ml ethanol solution. The solution was stirred for 10 min for complete dissolvation. Then, electrodes with similar area (8 cm^2) were placed in the solution. Nitrogen gas was purged into the electrolysis cell as a sweeping gas in order to omit dissolved oxygen. The process was continued for 2.5 h under constant voltage (30 V). Sky-blue precipitates which were a sign of $Cu_3(BTC)_2$ formation were collected by centrifugation and subsequently dried at 110 °C overnight. Finally, the MOF was activated at 150 °C for 3 h where the sky-blue precipitates turned to dark blue after activation. This phenomenon is due to the reduction in coordination number of Cu from six to four in complex state.

3. Characterization

The surface morphology and microstructures of the developed MOF were determined by field emission scanning electron microscopy (FE-SEM) analysis using Tescan instrument (MIRA3, Czech Republic) with 5 kV acceleration voltage. For conductivity purpose, the samples were gold sputtered before the analysis. Crystallinity, chemical composition and solid phase structure were studied by X-ray diffraction XRD analysis (X pert Pro, Panalytical, Germany), which is a non-destructive technique using monochromatic Cu-Kα radiation (λ=1.5406 A°) at 30 kV and 20 mA. The surface functional groups were detected by Fourier transform infrared (FTIR) spectroscopy (Bruker Vertex-70, Germany) using KBr pellet in the range of 400-4,000 cm^{-1}. The change in sample weight with respect to the temperature was measured by thermogravimetric analyzer (TGA) under air (oxidative) or nitrogen (inert) atmosphere (STA 1500, Rheometric Scientific, USA). This analysis was carried out to investigate the thermal stability of the samples. The BET surface area and microporous properties were calculated by nitrogen adsorption at 77 K over relative pressure range of 0.01 to 0.99 using a surface area analyzer (BELSORP-mini II, Japan).

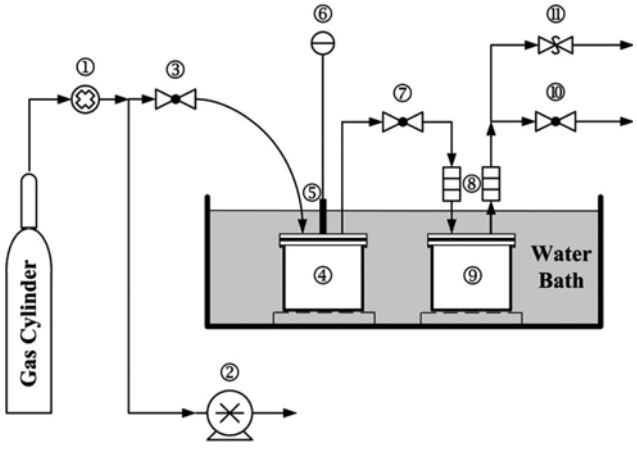

Fig. 2. Schematic diagram of volumetric gas adsorption set-up.

① Regulator
② Vacuum pump
③ Main valve
④ Load cell
⑤ Pressure transducer
⑥ Pressure indicator
⑦ Adsorption valve
⑧ Filter (inlet/outlet)
⑨ Adsorption cell
⑩ To vent
⑪ Metering valve

4. Gas adsorption Apparatus

Adsorption of pure gases was measured by volumetric method, which is one of the straightforward methods for gas adsorption. A schematic representation of the adsorption setup is shown in Fig. 2. The apparatus involved two stainless steel cells (load and adsorption cell) with the same volumes, which were kept at constant temperature using a water bath. The load cell was connected to the pressure indicator by pressure transmitter. Prior to each test, the whole system was degassed by vacuum pump. Then, the regulator and the main valve between gas cylinder and load vessel were opened and the gas flowed to the vessel till the pressure stabilized at the desired pressure. In the next step, the valve before adsorption cell was opened and the pressure distributed between the cells. Meanwhile, the pressure began to drop due to the adsorption of gas by MOF. Enough time was given to ensure that the equilibrium state was achieved and the final pressure was recorded. The adsorption amount of gases was calculated by material balance around the load and adsorption vessels, which could be considered as a closed system. This statement can be expressed by the following equation:

$$[N]_{p_1}+[N]_{a_1}=[N]_{p_2}+[N]_{a_2}+N_{ads} \quad (1)$$

where subscripts (p) and (a) indicate the pressure cell and adsorption cell, and subscripts 1 and 2 represent the initial state and final equilibrium state, respectively. N is the number of moles in each state which is obtained by real gas equation, N=(PV/ZRT), where V (m^3), P (Pa), T (K) and R (8.314 $Jmol^{-1}K^{-1}$) represent volume, pressure, temperature and the universal gas constant, respectively. Z denotes the compressibility factor which was calculated by Soave-Redlich-Kwong (SRK) equation of state. N_{ads} is the amount of adsorbed gas onto the sorbent (moles).

The gas adsorption experiments were carried out using high purity CO_2 (99.999%) and CH_4 (99.999%) at the pressure range of 0-22 bar and various temperatures (298, 308 and 318 K) which were provided by water bath. Finally, the adsorption capacity of $Cu_3(BTC)_2$ was calculated by SRK equation of state in MATLAB software (R2014b).

RESULTS AND DISCUSSION

1. Characterization Results

The XRD pattern of the electrochemically synthesized $Cu_3(BTC)_2$ is shown in Fig. 3 where all peaks corresponding to the reflection planes are indicated. The pattern is in good agreement with those available in the literature which were synthesized via solvothermal route. From Fig. 3, sharp diffraction peaks can be observed which show the highly crystalline nature of the synthesized MOF. The intensive peaks at low 2θ--, i.e. 9.6°, 11.8° and 40° can be attributed to (220), (222) and (400) crystal planes of $Cu_3(BTC)_2$, respectively [29]. Moreover, sharpness of mentioned peaks indicates the microporous nature of the developed $Cu_3(BTC)_2$ which possesses many small pores [30]. In electrochemical synthesis, there is a probability of copper oxide or copper dioxide formation due to the presence of water molecules in the solution; however, using ethanol as

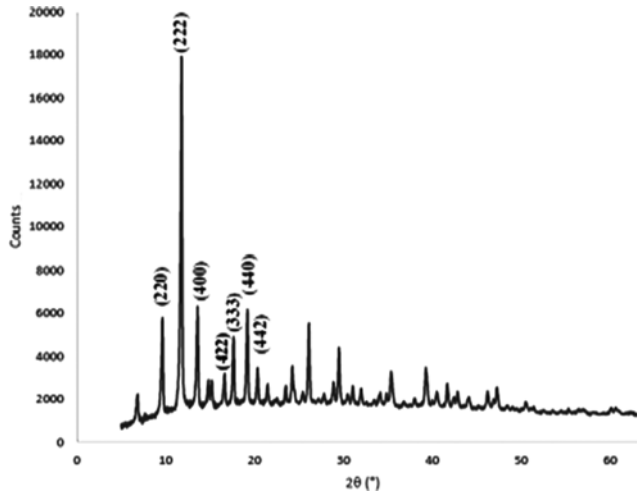

Fig. 3. XRD pattern of the electrochemically synthesized $Cu_3(BTC)_2$.

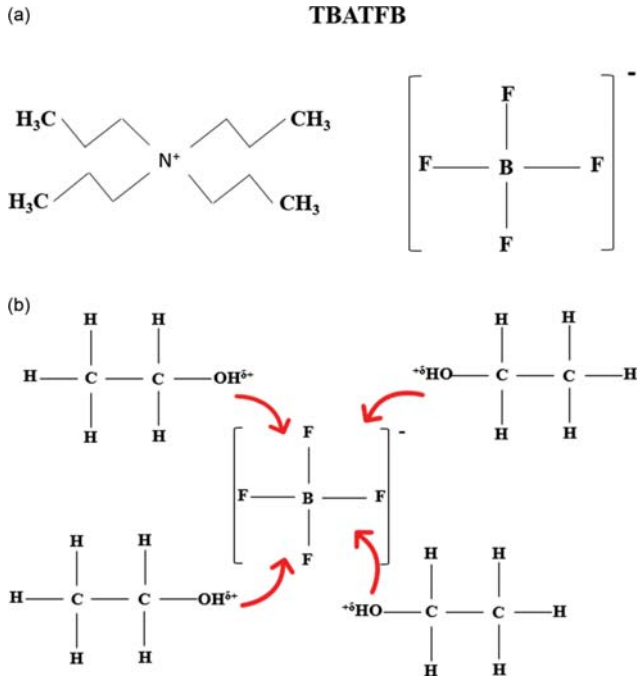

Fig. 4. (a) TBATFB chemical structure and (b) solvation of anionic part of TBATFB by ethanol molecules.

a solvent can diminish the formation of unwanted impurities in the medium since the polar segment of ethanol solves the anionic part of TBATFB (BF_4^-) [31-33] as depicted in Fig. 4. Consequently, this will cause an increase in solution conductivity, and no significant amount of copper oxide or copper dioxide will form in the medium.

Thus, as can be seen in Fig. 3 there was not any significant evidence of the existence of CuO (2θ=35.5°) and CuO_2 (2θ=36.43°) in the XRD pattern, which confirms the absence of the mentioned impurities [34].

The textural properties of the MOF were determined by adsorption of N_2 at 77 K, which is shown in Fig. 5. It is clear that

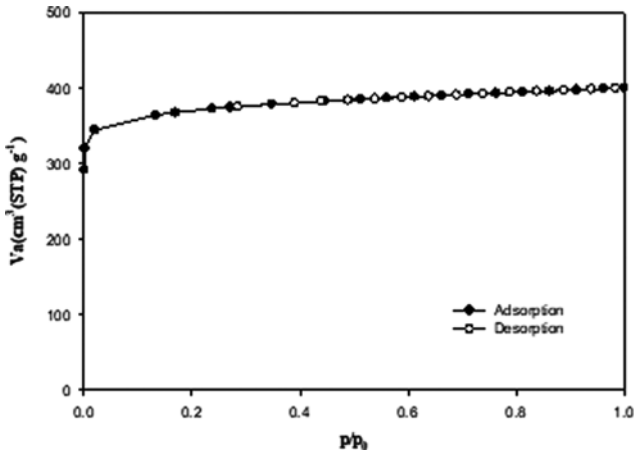

Fig. 5. N_2 adsorption-desorption isotherms on the developed $Cu_3(BTC)_2$ MOF.

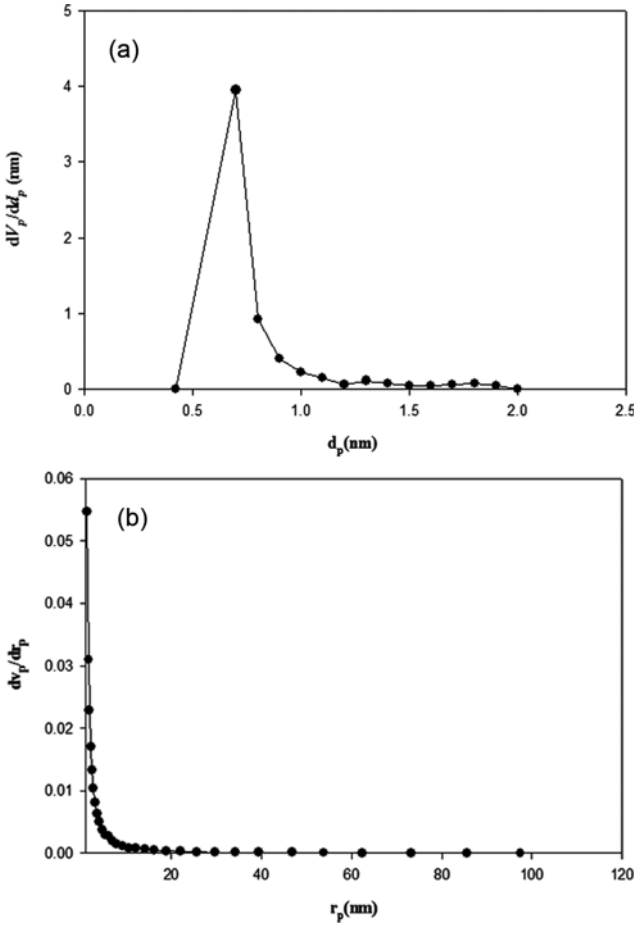

Fig. 6. (a) MP and (b) BJH plots of $Cu_3(BTC)_2$ MOF.

adsorption and desorption isotherms of nitrogen gas on electrochemically synthesized $Cu_3(BTC)_2$ completely overlapped and followed isotherm type I, which belongs to microporous materials according to the IUPAC classification.

Fig. 6 illustrates the pore size distribution of the synthesized $Cu_3(BTC)_2$ obtained from micropore (MP) and Barrett-Joyner-Hal-

Table 1. Textural properties of electrochemically synthesized $Cu_3(BTC)_2$ and those synthesized with other techniques

S_{BET} (m^2g^{-1})	Total pore volume ($cm^3\ g^{-1}$)	Micropore volume ($cm^3\ g^{-1}$)	Mean pore diameter (nm)	Ref.
1474.1	0.62	0.60	1.68	This work
452.2	0.28	N/A	N/A	[35]
708	0.48	N/A	N/A	[36]
1080	0.57	N/A	N/A	[37]
1370	0.57	0.48	1.67	[38]
1507	0.61	N/A	N/A	[39]
1119	0.59	N/A	N/A	[40]
1270	0.65	N/A	N/A	[40]

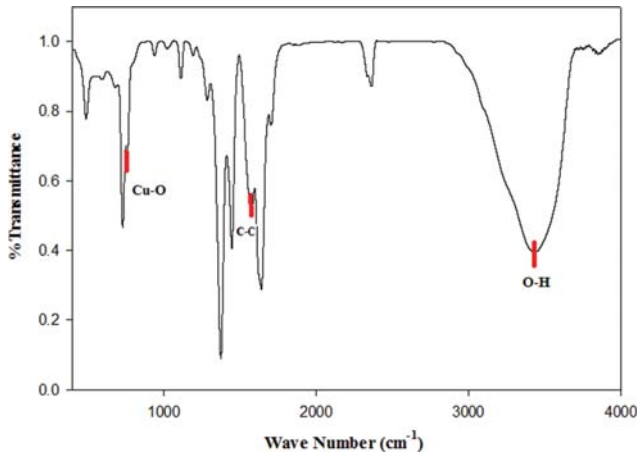

Fig. 7. FTIR spectrum of the synthesized $Cu_3(BTC)_2$.

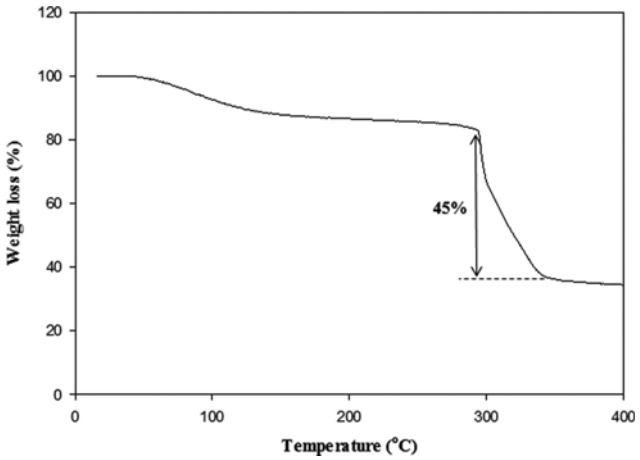

Fig. 8. Thermogravimetric curve of $Cu_3(BTC)_2$.

enda (BJH) methods. In Fig. 5 the majority of pores were distributed in the range of 0.42 to 1 nm, confirming that the as-synthesized MOF was highly microporous (more than 95% of the total pore volume). Detailed information about $Cu_3(BTC)_2$ structure including BET surface area, total pore volume, micropore volume and mean pore diameter is listed in Table 1, and meanwhile they are compared with similar studies reported for the synthesis of $Cu_3(BTC)_2$ through other techniques.

As indicated in Table 1, the as-synthesized $Cu_3(BTC)_2$ showed higher BET surface area and pore volume as opposed to most of studies, which confirms the reliability and effectiveness of electrochemical synthesis method. Furthermore, optimizing the electrochemical synthesis condition can improve the textural properties of final $Cu_3(BTC)_2$.

Fig. 7 shows the FTIR spectrum of the synthesized MOF. At the range of 1,500-1,600 cm^{-1}, symmetric COO stretches of the carboxylate group can be observed, which forms a complex with Cu^{+2}. This suggests that deprotonation in acidic C=O has occurred. The peak around 1,575 cm^{-1} can be assigned to C-C skeletal vibration of benzene groups in BTC linker. The sharp peak around 760 cm^{-1} is attributed to Cu-O stretching vibration, in which Cu is substituted on benzene groups by forming coordination bond with oxygen atom [41]. A broad band which can be observed in the region of 3,100-3,600 cm^{-1} is due to the presence of O-H in the coordinated polymer. As mentioned, there is no sign of the existence of CuO and Cu_2O crystals during the nucleation of $Cu_3(BTC)_2$; otherwise, some corresponding peaks should be observed at 410, 500, 610 and 615 cm^{-1} [42].

Fig. 8 illustrates thermo-gravimetric analysis of the MOF with weight loss when $Cu_3(BTC)_2$ is heated to 400 °C in the air. The first weight loss up to 150 °C corresponds to desorption of moisture or guest molecule which was physically adsorbed on the MOF. As can be seen, there was not any significant change in adsorbent weight up to 295 °C, which shows the high thermal stability of $Cu_3(BTC)_2$ at high temperatures and confirms the negligible amount of impurities in the structure. The second drastic mass drop (45%) happened around 295 °C due to the decomposition of the ligand (1,3,5 Benzentricarboxylate acid) and the remaining was copper oxide (CuO). Therefore, prior to adsorption tests it was necessary to regenerate $Cu_3(BTC)_2$ near its regeneration temperature (150 °C) to remove moisture and adsorbed gases from its surface [30].

The morphology and the particle shape of electrochemically synthesized $Cu_3(BTC)_2$ was studied by FE-SEM analysis as shown in Fig. 9. Octahedral shape of $Cu_3(BTC)_2$ is clearly obvious from Fig. 9, which is highly similar to those synthesized through solvothermal method [29,41].

2. Adsorption Experiments

To investigate the gas adsorption performance of the electrochemically synthetized $Cu_3(BTC)_2$, CO_2 and CH_4 adsorption experiments were carried out at different pressures, and the results were expressed by physical models to describe the equilibrium uptake.

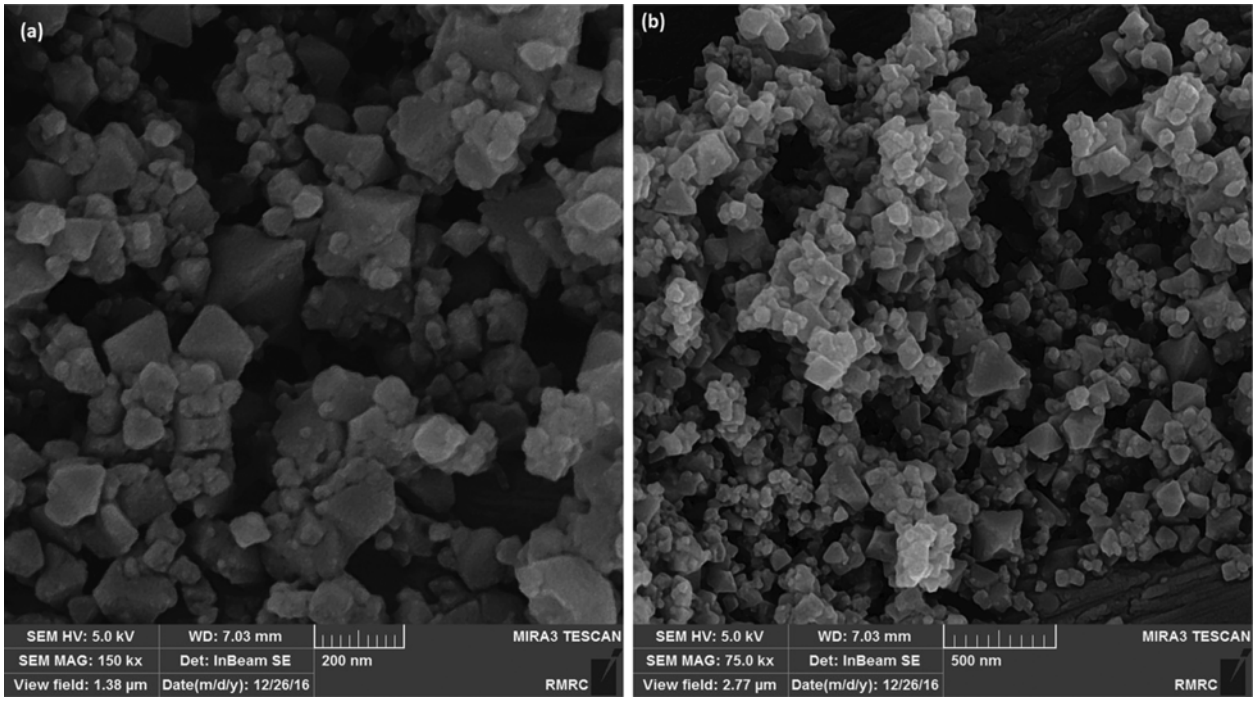

Fig. 9. FE-SEM micrographs of the synthesized $Cu_3(BTC)_2$ at different magnifications (a) 200 nm and (b) 500 nm.

There are several isotherm models which can be used for this purpose, among which Langmuir and Sips isotherms are more appropriate for gas adsorption. Langmuir model can be expressed as follows:

$$\text{Langmuir: } q_e = q_m \frac{K_L P}{1 + K_L P} \tag{2}$$

where q_e is the adsorption capacity (mmol g^{-1}) at equilibrium pressure P; q_m is the maximum amount of gas adsorbed (mmol g^{-1}) and K_L (bar^{-1}) is the Langmuir constant.

Sips isotherm model is a three-parameter model that is a combination of Langmuir and Freundlich isotherm models. In most gas adsorption studies, the Sips model gives more realistic prediction by considering ideal/non ideal interactions between adsorbate and adsorbent surface [43]:

$$\text{Sips: } q_e = q_m \frac{(K_s P)^{1/n}}{1 + (K_s P)^{1/n}} \tag{3}$$

where q_m (mmol g^{-1}) is the amount of gas adsorbed, K_s (bar^{-1}) is the Langmuir type constant and n is heterogeneity parameter.

Nonlinear fit of carbon dioxide and methane uptake at equilibrium condition and three different temperatures of 298, 308 and 318 K is shown in Fig. 10. $Cu_3(BTC)_2$ had preferential adsorption tendency toward CO_2 over CH_4. Since the cage diameter of $Cu_3(BTC)_2$ is approximately 0.9 nm, the size exclusion phenomenon cannot be the mechanism for CO_2/CH_4 separation, since these molecules have small kinetic diameters (0.33 and 0.38 nm, respectively) that can pass easily through the pores. Higher adsorption of CO_2 might have occurred due to the extra contribution from binding between CO_2 and open metal sites, which is stronger than other interactions such as van der Waals type existing between CH_4 molecules

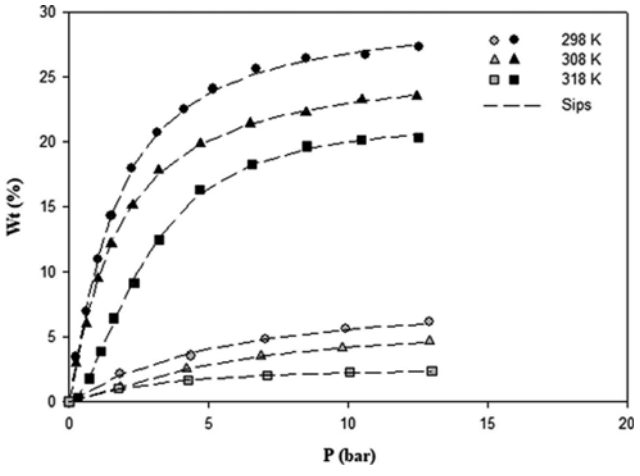

Fig. 10. Adsorption isotherms of CO_2 (black symbols) and CH_4 (grey symbols) at different temperatures on $Cu_3(BTC)_2$.

and the adsorbent surface. In fact, the existence of metal ions brings an enhanced electrostatic interaction between CO_2 quadrupole moment and open metal charge (thermodynamic separation) [44]; however, nonpolar nature of methane molecules provides less interaction with unsaturated, accessible metal sites [35]. Therefore, the difference in physical property of gas molecules (CO_2 and CH_4) determined the amount of adsorption. Table 2 compiles the adsorption constants of Langmuir and Sips isotherm models. It is clear that the Sips isotherm model fitted the equilibrium data quite well for both CO_2 and CH_4 (high R^2) in comparison to the Langmuir model. This means that at low pressure range, the Freundlich isotherm model was dominant, and at higher pressure monolayer

Table 2. Langmuir and Sips isotherm constants for CO_2 and CH_4 adsorption on $Cu_3(BTC)_2$

	CO_2			CH_4		
Temperature (K)	298	308	318	298	308	318
Langmuir						
q_m (mmol g^{-1})	31.830	27.546	23.578	8.635	7.005	2.710
K_L (bar^{-1})	0.5406	0.5223	0.1733	0.1774	0.1365	0.3757
R^2	0.9954	0.9978	0.9726	0.9958	0.9927	0.9734
Sips						
q_m (mmol g^{-1})	29.230	26.040	21.160	8.218	5.703	2.677
K_s (bar^{-1})	0.6224	0.5920	0.3716	0.1967	0.2020	0.3579
1/n	1.202	1.134	1.812	1.091	1.452	1.238
R^2	0.9988	0.9993	0.9991	0.9912	0.9985	0.9944

Table 3. Comparison of CO_2 or CH_4 uptake by different types of MOFs

Adsorbent	CO_2 uptake (mmol g^{-1})	CH_4 uptake (mmol g^{-1})	P (bar)	Temperature (K)	Reference
ZIF-7	2.75	0.12	1	298	[46]
MIL-125 (Ti)	3.80	0.95	10	298	[47]
HKUST-1	5.45	0.82	10	298	[35]
HKUST-1	3.63	-	1	298	[36]
HKUST-1	7.56	-	5	298	[37]
MIL-53	2.27	-	1	296	[48]
MIL-96	4.10	-	1	296	[48]
Zn(II) MOF	1.23	0.15	1	298	[49]
$Cu_3(BTC)_2$	8.12	4.10	10	298	This work

adsorption (Langmuir isotherm model) occurred, signifying that the adsorbent reached its saturation region. In this case, the Freundlich isotherm model was unable to fit the equilibrium data at low pressures since this model is applied when there is high affinity for the adsorbent and consequently, the initial slope is very high. On the other hand, at higher pressures the adsorption behavior reached to asymptotic plateau; while, if equilibrium data follow Freundlich isotherm model, the adsorbent does not show clearly limited adsorption capacity [45].

The maximum adsorption capacity of $Cu_3(BTC)_2$ for CO_2 and CH_4 was 8.42 and 4.43 mmol g^{-1} at 298 K, respectively, which is comparable with results obtained from other MOFs synthesized by conventional routes like solvothermal or hydrothermal methods. Table 3 compares some recent progress in adsorption of CO_2 or CH_4 using different kinds of MOFs.

As can be seen from Table 3, the amount of CO_2 and CH_4 uptake by the electrochemically synthesized $Cu_3(BTC)_2$ in the present study was comparable and in most cases even higher than those which were synthesized by solvothermal route.

3. Kinetic Study

Adsorption kinetics is a significant factor for estimating the performance of fixed bed or any other flow-through system [50]. There are two main classes of theoretical models that have been proposed to describe adsoption data: adsorption reaction models and adsorption diffution models. Although both models are used to define the adsorption kinetics, they are completely different. Adsorption diffusion refers to three consecutive processes, i.e. film diffusion, internal diffusion and mass diffusion, while the adsorption reaction is based on chemical reaction kinetics and covers the whole process of adsorption [51].

Pseudo-first-order and pseudo-second-order are the most common adsorption kinetic models which are applied to describe adsorption kinetics and adsorbate-adsorbent interactions. Pseudo-first-order model predicts physical adsorption, which is usually reversible. However, the main assumption of pseudo-second-order is chemical interactons which are usually formed by strong bonds between adsorbates and adsorbent [52]. Pseudo-first and pseudo-second order kinetic models are as follows:

$$q_t = q_e(1 - e^{k_1 t}) \tag{4}$$

$$q_t = \frac{k_2 q_e^2}{1 + k_2 q_e t} t \tag{5}$$

where k_1 (s^{-1}) and k_2 ($g \cdot mmol^{-1} \cdot s^{-1}$) are rate constants, q_t (mmol·g^{-1}) and q_e are adsorption capacity at time t and equilibrium, respectively.

It would be more convenient to choose the order of the adsorption reaction as an adjustable parameter. In this study, pseudo-*n*th order kinetic model was used to calculate the order of reaction directly [52]. This equation can be presented as follows:

$$q_t = q_e - [(q_e)^{1-n} + (n-1)K_n t]^{1/1-n} \tag{6}$$

where q_t (mmol·g^{-1}) and q_e are adsorption capacity at time t and equilibrium, respectively, K_n (s^{-1}) is the rate constant and n is the order of reaction.

Fig. 11 depicts the adsorption kinetics of CO_2 and CH_4 on

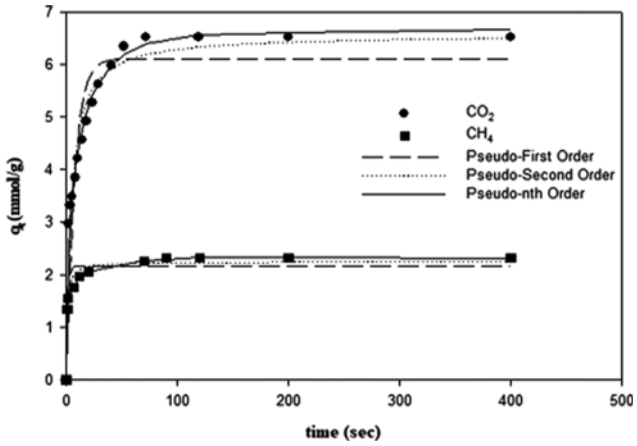

Fig. 11. CO_2 and CH_4 adsorption kinetics at 298 K and 8 bar.

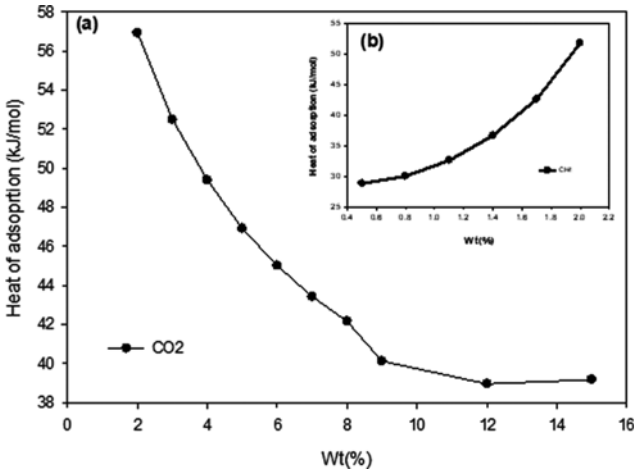

Fig. 12. Isosteric heat of adsorption against surface coverage for (a) CO_2 and (b) CH_4.

$Cu_3(BTC)_2$ at 298 K and 8 bar. It is clear that the adsorption was very rapid at the early stage of the process until reaching its highest uptake and then approached to a plateau form, indicating that the adsorbent was saturated by gas molecules. This behavior can be observed for both CO_2 and CH_4 molecules. Sharp increase in the adsorption capacity at the beginning of the process is due to the vacant and unsaturated active sites which are available for the adsorbates. After a while, the number of accessible sites decreased, and at the equilibrium the amount of uptake became almost constant. As can be observed in Fig. 10, carbon dioxide needed more time to attain its equilibrium state in comparison to methane. This can be attributed to the molecular weight of CO_2 which is heavier than CH_4; thus, CO_2 mobility would be restricted in gas space. Furthermore, small surface diffusivity of CO_2 is another reason that causes slow movement of CO_2 molecules towards the inner pores [53].

The kinetic parameters obtained through non-linear fit of experimental data are summarized in Table 4.

As can be seen from Table 4, pseudo-first-order and second-order models could not fit the experimental data very well; however, the *n*th-order model predicted the kinetic behavior with high accuracy. Since the values of adjusted parameter for both gases were close to 1, this implies that the adsorption process was controlled by strong physisorption mechanism.

4. Adsorption Thermodynamic

Isosteric heat (ΔH_{st}) is the key parameter for determining the thermal nature of the process. This parameter is defined by the Clausius-Clapeyron equation:

$$\Delta H_{st} = R\frac{d\ln P}{d\left(\frac{1}{T}\right)_{q_e}} \quad (7)$$

To calculate the heat of adsorption, the amount of gas uptake at different temperatures was used. Fig. 12 depicts the isosteric heat of adsorption of CO_2 and CH_4 on $Cu_3(BTC)_2$ versus the amount of uptake. The high value of ΔH_{st} (56.93 kJ mol^{-1}) for CO_2 at the beginning of the process is due to the direct interaction of adsorbate and adsorbent surface which led to the release of large adsorption heat. As the adsorbent sites were occupied by CO_2 molecules, the heat of adsorption decreased consistently and monotonically due to the weak contact between gas molecules and adsorbent surface. However, this trend for methane was completely opposite. The isosteric heat of adsorption (28.46 kJ mol^{-1}) increased gradually as the surface coverage increased. This phenomenon occurs due to the enhanced intermolecular forces among molecules at higher surface loadings [54,55].

As can be seen in Fig. 12, the heat of adsorption of CO_2 is higher than CH_4 due to the geometrical shape of gas molecules. Since CO_2 molecule has a claviform shape, it will be affected more by the pore wall than CH_4 molecule which has regular tetrahedral shape; therefore, it produces more energy and heat [56].

5. Ideal Adsorption Solution Theory (IAST)

Ideal adsorption solution theory (IAST), first proposed by Myers and Praunitz [57], has been widely applied to predict the adsorption selectivity and mixed gas adsorption using isotherms of pure components. This model assumes that the adsorbed gas mixture behaves like an ideal solution at constant spreading pressure and temperature, i.e., all components in the mixture follow a rule similar to Raoult's law [58]. In the present study, IAST was employed to predict CO_2/CH_4 binary mixture adsorption. The adsorption selectivity for a binary gas mixture is defined as follows:

Table 4. Constants of kinetic models for adsorption of CO_2 and CH_4 on $Cu_3(BTC)_2$

	Pseudo- first order				Pseudo- second order			Pseudo-*n*th order			
	$q_{e\,(exp)}$	k_1	$q_{e\,(cal)}$	R^2	k_2	$q_{e\,(cal)}$	R^2	$q_{e\,(cal)}$	K_n	n	R^2
CO_2	6.71	0.1366	6.11	0.8749	0.0338	6.57	0.9529	6.590	0.0453	1.29	0.9857
CH_4	2.31	0.7886	2.16	0.9251	0.5107	2.25	0.9720	2.305	0.6512	1.16	0.9986

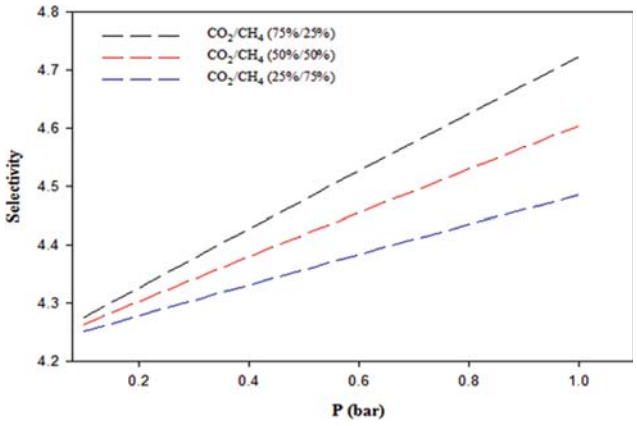

Fig. 13. IAST predicted selectivities for different CO_2/CH_4 compositions adsorbed on $Cu_3(BTC)_2$ at 298 K.

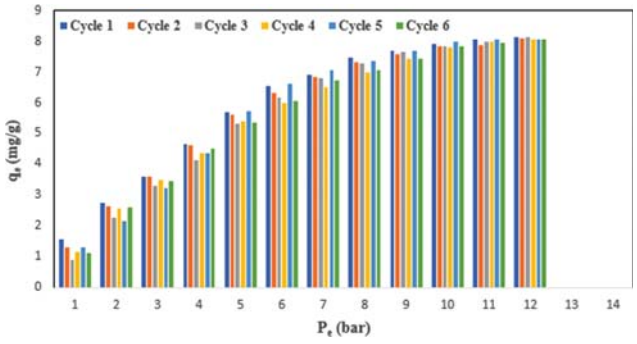

Fig. 14. Cyclic performance of $Cu_3(BTC)_2$ over several cycles of CO_2 adsorption-desorption at 298 K.

$$S = \frac{x_1/x_2}{y_1/y_2} \quad (8)$$

where x is the mole fraction in adsorbed phase and y is the mole fraction in gas phase.

Fig. 13 shows the selectivity of CO_2/CH_4 at different gas mixture compositions. As it is clear, with increase in gas mixture pressure or CO_2 mole fraction (heavier component), selectivity increases. This can be attributed to the lateral interactions between CO_2 molecules that were enhanced as the mixture pressure increased [59].

6. Assessment of $Cu_3(BTC)_2$ Regenerability in Sequential Cycles

From a practical point of view, the stability of an adsorbent to sustain its adsorption capacity is one of the important parameters that must be considered. Fig. 14 represents the adsorption-desorption profiles of CO_2 in six consecutive adsorption-desorption runs. The duration of each sorption-desorption cycle for $Cu_3(BTC)_2$ was 24 h. As seen in Fig. 14, the as-synthesized MOF exhibited acceptable cyclic performance and kept its maximum adsorption capacity after six cycles (~8.42 mmol g^{-1} at 12.5 bar).

CONCLUSION

We demonstrated that electrochemical synthesis can be a convenient approach with high efficiency (yield about 80%) for synthesis of $Cu_3(BTC)_2$ MOF at ambient conditions. Results obtained from various analyses confirmed the high textural properties, high crystallinity and good thermal stability of the aforementioned MOF. The amount of CO_2 and CH_4 uptake was satisfactory and competitive with those reported for other MOFs synthetized through other routes. The prediction based on IAST also demonstrated that $Cu_3(BTC)_2$ can adsorb CO_2 more selectively than CH_4 at higher CO_2 mole fractions. Also, the potential of the adsorbent in keeping its adsorption capacity was examined through six sequential cycles and no significant loss was observed in CO_2 uptake, which confirms that the electrochemically synthetized $Cu_3(BTC)_2$ had good stability in repeated adsorption runs.

Although, numerous MOFs with high gas adsorption capacities were developed via other routes such as solovothermal, the results of the present study demonstrated that the electrochemical method offers some outstanding advantages over the traditional routes which are (i) operating at ambient conditions (i.e., low energy consumption), (ii) completeion of synthesis in short period of time, and (iii) no need for metal salt, which means that one chemical compound is omitted. Therefore, MOFs can be a suitable substitution for conventional adsorbents due to their special characteristics, and they can be used in packed columns for capturing hazardous components before being emitted to the atmosphere.

REFERENCES

1. H. R. Abid, Z. H. Rada, J. Shang and S. Wang, *Polyhedron* (2016).
2. C. Stewart and M.-A. Hessami, *Energy Convers. Manage.*, **46**, 403 (2005).
3. A. K. Adhikari and K.-S. Lin, *Chem. Eng. J.*, **284**, 1348 (2016).
4. H. C. Yoon, P. B. S. Rallapalli, S. S. Han, H. T. Beum, T. S. Jung, D. W. Cho, M. Ko and J.-N. Kim, *Korean J. Chem. Eng.*, **32**, 2501 (2015).
5. Y. He, W. Zhou, G. Qian and B. Chen, *Chem. Soc. Rev.*, **43**, 5657 (2014).
6. M. G. Waller, E. D. Williams, S. W. Matteson and T. A. Trabold, *Appl. Energy*, **127**, 55 (2014).
7. S. Choi, J. H. Drese and C. W. Jones, *ChemSusChem*, **2**, 796 (2009).
8. X. Wang, L. Chen and Q. Guo, *Chem. Eng. J.*, **260**, 573 (2015).
9. Y. Li, H. Yi, X. Tang, F. Li and Q. Yuan, *Chem. Eng. J.*, **229**, 50 (2013).
10. L. Liu, D. Nicholson and S. K. Bhatia, *J. Phys. Chem. C*, **119**, 407 (2014).
11. H. Yi, F. Li, P. Ning, X. Tang, J. Peng, Y. Li and H. Deng, *Chem. Eng. J.*, **215**, 635 (2013).
12. C. Shen, C. A. Grande, P. Li, J. Yu and A. E. Rodrigues, *Chem. Eng. J.*, **160**, 398 (2010).
13. F. Raganati, V. Gargiulo, P. Ammendola, M. Alfe and R. Chirone, *Chem. Eng. J.*, **239**, 75 (2014).
14. K. Munusamy, G. Sethia, D. V. Patil, P. B. S. Rallapalli, R. S. Somani and H. C. Bajaj, *Chem. Eng. J.*, **195**, 359 (2012).
15. C. Janiak and J. K. Vieth, *New J. Chem.*, **34**, 2366 (2010).
16. A. Martinez Joaristi, J. Juan-Alcañiz, P. Serra-Crespo, F. Kapteijn and J. Gascon, *Cryst. Growth Des.*, **12**, 3489 (2012).
17. J. R. Long and O. M. Yaghi, *Chem. Soc. Rev.*, **38**, 1213 (2009).
18. H. Al-Kutubi, J. Gascon, E. J. Sudhölter and L. Rassaei, *ChemElec-*

troChem, **2**, 462 (2015).
19. D.-W. Jung, D.-A. Yang, J. Kim, J. Kim and W.-S. Ahn, *Dalton Trans.*, **39**, 2883 (2010).
20. Z. Ni and R. I. Masel, *J. Am Chem. Soc.*, **128**, 12394 (2006).
21. S. Khazalpour, V. Safarifard, A. Morsali and D. Nematollahi, *RSC Adv.*, **5**, 36547 (2015).
22. R. Ameloot, L. Stappers, J. Fransaer, L. Alaerts, B. F. Sels and D. E. De Vos, *Chem. Mater.*, **21**, 2580 (2009).
23. A. U. Czaja, N. Trukhan and U. Müller, *Chem. Soc. Rev.*, **38**, 1284 (2009).
24. S. S.-Y. Chui, S. M.-F. Lo, J. P. Charmant, A. G. Orpen and I. D. Williams, *Science*, **283**, 1148 (1999).
25. K. Schlichte, T. Kratzke and S. Kaskel, *Micropor. Mesopor. Mater.*, **73**, 81 (2004).
26. M. Gaab, N. Trukhan, S. Maurer, R. Gummaraju and U. Müller, *Micropor. Mesopor. Mater.*, **157**, 131 (2012).
27. P. Silva, S. M. Vilela, J. P. Tomé and F. A. A. Paz, *Chem. Soc. Rev.*, **44**, 6774 (2015).
28. A. Grondein and D. Bélanger, *Fuel*, **90**, 2684 (2011).
29. S. Khoshhal, A. A. Ghoreyshi, M. Jahanshahi and M. Mohammadi, *RSC Adv.*, **5**, 24758 (2015).
30. B. Sun, S. Kayal and A. Chakraborty, *Energy*, **76**, 419 (2014).
31. T. M. Letcher, *Thermodynamics, solubility and environmental issues*, Elsevier (2007).
32. B. Wu, Y. Zhang and H. Wang, *J. Phys. Chem. B*, **113**, 12332 (2009).
33. W. Caminati, S. Melandri, A. Maris and P. Ottaviani, *Angew. Chem. Int. Ed.*, **45**, 2438 (2006).
34. M. Hartmann, S. Kunz, D. Himsl, O. Tangermann, S. Ernst and A. Wagener, *Langmuir*, **24**, 8634 (2008).
35. J. Li, J. Yang, L. Li and J. Li, *J. Energy Chem.*, **23**, 453 (2014).
36. F. Martínez, R. Sanz, G. Orcajo, D. Briones and V. Yángüez, *Chem. Eng. Sci.*, **142**, 55 (2016).
37. S. Bhadauria, A. Nanoti, S. Dasgupta, S. Divekar, P. Gupta and R. Chauhan, *RSC Adv.*, **6**, 93003 (2016).
38. S. Salehi and M. Anbia, *Energy Fuels*, **31**, 5376 (2017).
39. N. Al-Janabi, P. Hill, L. Torrente-Murciano, A. Garforth, P. Gorgojo, F. Siperstein and X. Fan, *Chem. Eng. J.*, **281**, 669 (2015).
40. M. Schlesinger, S. Schulze, M. Hietschold and M. Mehring, *Micropor. Mesopor. Mater.*, **132**, 121 (2010).
41. R. S. Kumar, S. S. Kumar and M. A. Kulandainathan, *Micropor. Mesopor. Mater.*, **168**, 57 (2013).
42. I. Ardelean and S. Cora, *J. Mater. Sci.: Mater. Electronics*, **19**, 584 (2008).
43. F. Banisheykholeslami, A. A. Ghoreyshi, M. Mohammadi and K. Pirzadeh, *CLEAN-Soil, Air, Water*, **43**, 1084 (2015).
44. H. Wu, J. M. Simmons, G. Srinivas, W. Zhou and T. Yildirim, *J. Phys. Chem. Lett.*, **1**, 1946 (2010).
45. G. Limousin, J.-P. Gaudet, L. Charlet, S. Szenknect, V. Barthes and M. Krimissa, *Appl. Geochem.*, **22**, 249 (2007).
46. C. Zhu, Z. Zhang, B. Wang, Y. Chen, H. Wang, X. Chen, H. Zhang, N. Sun, W. Wei and Y. Sun, *Micropor. Mesopor. Mater.*, **226**, 476 (2016).
47. Z. H. Rada, H. R. Abid, J. Shang, Y. He, P. Webley, S. Liu, H. Sun and S. Wang, *Fuel*, **160**, 318 (2015).
48. H. R. Abid, Z. H. Rada, J. Shang and S. Wang, *Polyhedron*, **120**, 103 (2016).
49. J. Du and G. Zou, *Inorg. Chem. Commun.*, **69**, 20 (2016).
50. H. Qiu, L. Lv, B.-c. Pan, Q.-j. Zhang, W.-m. Zhang and Q.-x. Zhang, *J. Zhejiang University-Science A*, **10**, 716 (2009).
51. N. Lazaridis and D. Asouhidou, *Water Res.*, **37**, 2875 (2003).
52. E. Mehrvarz, A. A. Ghoreyshi and M. Jahanshahi, *Front. Chem. Sci. Eng.*, **11**, 252 (2017).
53. I. Prasetyo and D. Do, *Chem. Eng. Sci.*, **53**, 3459 (1998).
54. S. Chowdhury and R. Balasubramanian, *J. CO_2 Util.*, **13**, 50 (2016).
55. Z. Bao, L. Yu, Q. Ren, X. Lu and S. Deng, *J. Colloid Interface Sci.*, **353**, 549 (2011).
56. H. Zhimin, Y. Guocong and D. Barba, *J. Chem. Ind. Eng. (China)*, **44**, 143 (1993).
57. A. Myers and J. M. Prausnitz, *AIChE J.*, **11**, 121 (1965).
58. Z. Zhang, S. Xian, Q. Xia, H. Wang, Z. Li and J. Li, *AIChE J.*, **59**, 2195 (2013).
59. P. Mishra, S. Mekala, F. Dreisbach, B. Mandal and S. Gumma, *Sep. Purif. Technol.*, **94**, 124 (2012).